Lasers in Manufacturing Conference 2021

Laser powder bed fusion of pure copper using a 1000 W green laser

G. Nordet[a,b,*], C. Gorny[b], P. Lapouge[b], A. Effernelli[a], E. Blanchet[a], F. Coste[b] and P. Peyre[b]

[a] *ADDUP, 5 Rue Bleue, 63118 Cébazat, France*
[b] *PIMM Laboratory, Arts et Métiers Institute of Technology, CNRS, CNAM, HESAM University 151 Bd de l'Hôpital, 75013 PARIS*

Abstract

Additive manufacturing of copper is still considered as complex using the usual IR laser wavelength. For the L-PBF process, the density of copper parts stays at an average value of less than 99 %. These low densities of parts could be explained by the high reflectance at IR wavelength and the high conductivity of pure copper, which necessitates using more power than other materials. In this context, changing the laser wavelength from near IR to green, with the recently developed industrial sources, allows to improve the laser-matter interaction and reduce the power needed to satisfactorily densify copper. In the current study, we demonstrate the possibility to implement a 1000 W green laser on a dedicated L-PBF test bench using a 15-45 µm pure copper powder. A parametric study is then carried out to create dense parts. Such an innovative work allows creating up to 99.9 % dense parts of pure copper which is much better than all the recent investigations using IR laser sources.

Keywords: Type your keywords here, separated by semicolons ;

1. Introduction

Pure copper, due to its high thermal and electrical conductivity, is a widely used material in the electronics and power production sectors. Such applications need to combine complex parts geometry and elevated electrical conductivity. Additionally, the combination of complex geometry – highly IR reflective and conductive materials is also a key point for other fields such as the jewelry industry. Additive Manufacturing (AM) is an adequate answer to the need for the new design. More precisely, the high precision and resolution

* Corresponding author.
E-mail address: guillaume.nordet@ensam.eu

provided by Laser Powder Bed Fusion (L-PBF) is a good candidate to manufacture very complex forms and reduce the waste of materials during the process.

However, porosity is highly detrimental to electrical conductivity. Existing studies on L-PBF of pure copper using IR wavelengths have shown that a maximum of 98.5 % parts density is obtained using very high energy density (Colopi et al., 2018; Jadhav et al., 2020; Lykov et al., 2016) or new building strategies (Colopi et al., 2019). For this reason, the usual IR (1.07 µm) L-PBF technology still exhibits limitations to obtain fully dense pure copper. The infrared wavelength usually used in the L-PBF system is not well absorbed by pure copper (around 5 % in solid-state), causing several damages to the laser optics (S. D. Jadhav et al., 2019) due to back reflections. Moreover, using high energy density to counterbalance power reflections seems to be detrimental to the L-PBF process, due to severe spattering effects.

Some solutions have been developed to reduce the energy density needed to create dense parts. Among those solutions, changing the material to make it more absorbent seems to be the easier one. As an example, (Jadhav, 2019) (S. D. Jadhav et al., 2019) show that slight oxidation of powder allows obtaining as dense and conductive parts halving the energy density. Similarly, adding some carbon particles to the powder allows for reducing the needed energy (Jadhav et al., 2019).

The use of recently developed green lasers has already shown a better coupling with copper for welding applications (Engler et al., 2011; Haubold et al., 2018; Heider et al., 2011). Indeed, the green wavelength (λ = 532 or 515 nm) is more absorbed by pure copper at solid and liquid states. Corresponding absorption rates were shown to be comprised between 40% (Engler et al., 2011) for solid-state and 25 % at a liquid state. Consequently, the use of green laser is expected to allow reducing by a factor 2 the power needed to have similar penetration depths (Kaiser et al., n.d.).

In this work, we study the possibility to densify pure copper using a 1 kW TRUMPF green laser, already tested for welding applications (Haubold et al., 2018; Kaiser et al., n.d.), and implemented on an L-PBF test. A global parametric study is carried out, ranging from single L-PBF tracks to cubic 3D parts.

2. Experimental setup

2.1. L-PBF Test bench

The test bench is an opened and instrumented L-PBF machine in which the green laser TRUMPF 1kW was specifically adapted (Fig.1). The L-PBF machine consists of two pistons and a polymer scrapper to feed and spread the powder. All the axes and laser trigger were controlled by an Aerotech program, which communicates with the TruControl interface.

The laser used is the commercial green laser TruDisk 1020 with 1 kW cw output power. The spatial distribution is nearly top-hat, with a minimum diameter of 90 µm at the focus distance of ≈170 mm (rather short compared with usual IR L-PBF machines). To limit the impact of ejections and metal vapor, two argon cross-jet are set one at 1-2 cm above the powder-bed level to remove spatters, the second one is near the external window level, to protect it from metallic vapors.

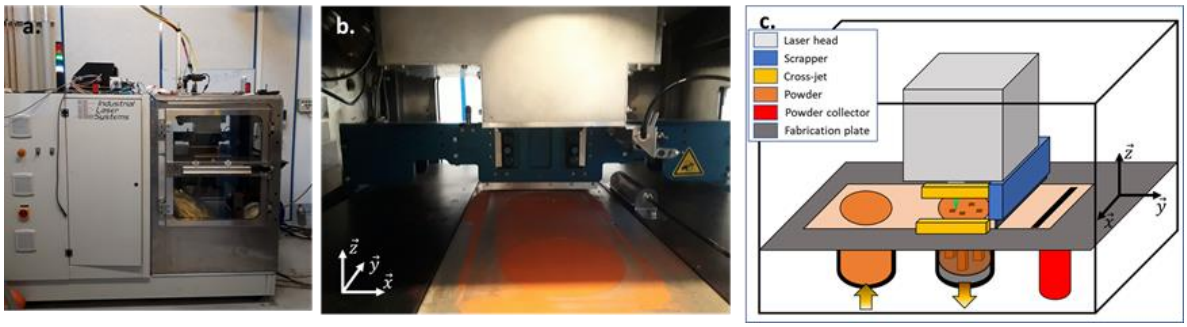

Fig. 1. Experimental setup. (a) L-PBF test bench equipped with TruDisk 1020 1kW green laser source; (b) View of the building area; (c) schematic of the test bench.

2.2. Powder and substrate

A 15-45 µm gas atomized powder of pure copper was used as starting material. After each fabrication, the used powder is recuperated and sifted using a 63 µm sieve. The powder is automatically reused for the next fabrication and reintroduced in the feeding piston.

For the different experimental conditions, two types of substrates are used.

- For single L-PBF tracks: a plate of pure copper of 1 mm thickness. Only for those experiments, the powder was manually spread. Powder thickness was estimated to 70 µm +/- 10 µm and the compacity average value is near 40 % +/- 5%.
- For 3D parts: a 150 mm diameter 316L platform. All 3D parts are built using 3 mm supports to easily separate parts from the platform and limit the copper–steel dilution.

2.3. Experimental procedure

As indicated above, for the validation of a green wavelength applied to the L-PBF process, two steps have been considered:

- First, single tracks have been considered for a large range of power/scan speed values, to address the geometry and stability range of fusion tracks on P versus V maps. Such a first approach also allows estimating adequate hatch distances through the measurement of track's widths and provides a deeper understanding of green laser-pure copper coupling.
- Second, 3D cubic parts of 10 mm edge have been manufactured, using different layer thickness and (P, V, hatch) conditions with the main objective of optimizing parts density. The density of parts was analyzed using image analysis carried out on optical micrographs captured at a x 200 magnification.

3. Results and discussion

3.1. Analysis of single L-PBF tracks

The analysis of single L-PBF tracks is expected to allow reducing the number of L-PBF 3D parts during the optimization step, by making a first and fast classification of more adequate (P, V) conditions. Four parameters are mainly addressed: (1) the continuity of the track, (2) the track width (L), (3) the track's depth e of the track, and L_T the total width, including the track width and the two denudation widths around the L-PBF track.

Corresponding data are systematically obtained using optical microscopy.

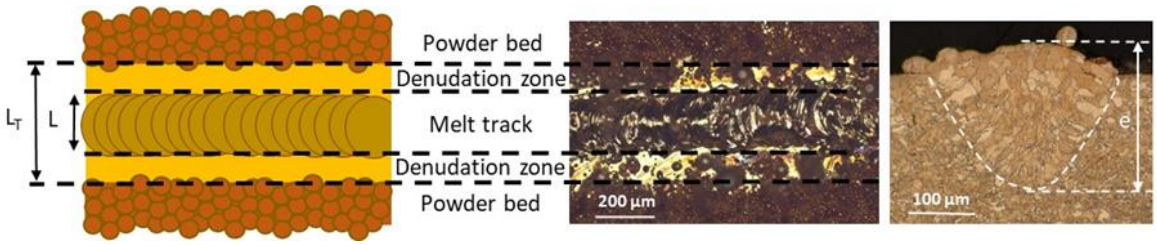

Fig. 2. Main parameters considered in the single tracks' analysis.

- Continuity

To obtain dense parts, and favor an optimum overlap between adjacent tracks, the track's continuity-stability is an important aspect. Four stability domains could be determined on a P-V map, following previous works (Gunenthiram et al., 2017).

- The Balling domain: powder just spheroidized. Not any over-melting of the previous layer that could not provide to the creation of dense parts. Moreover, those spheres do not screech to the under the substrate and just be deleted by the next scraper passage. Those conditions must be avoided in red on fig.3(a) and the upper view on fig.3(c).
- Partly continuous tracks: That constitutes a limit between the continuous track and balling. Tracks are mostly continuous with local discontinuities. There is just enough energy to melt the substrate below the powder layer. Those conditions are represented on the upper view in fig3(d) and by the hollow green circles in fig 3(a).
- Humping: The humping, already described by (Tang, 2020) (Tang, 2020) is a condition for which the convective movements of the melt pool cause it to form humps and valleys. More specifically, the occurrence of humps, may cause powder height variations and induce lacks of fusion. Considering the predominance of humping at 1 m/s, it can be assumed that the maximum scan speed for 3D parts would be near 0.8 m/s.
- Continuous tracks: optimum conditions to create a dense part.

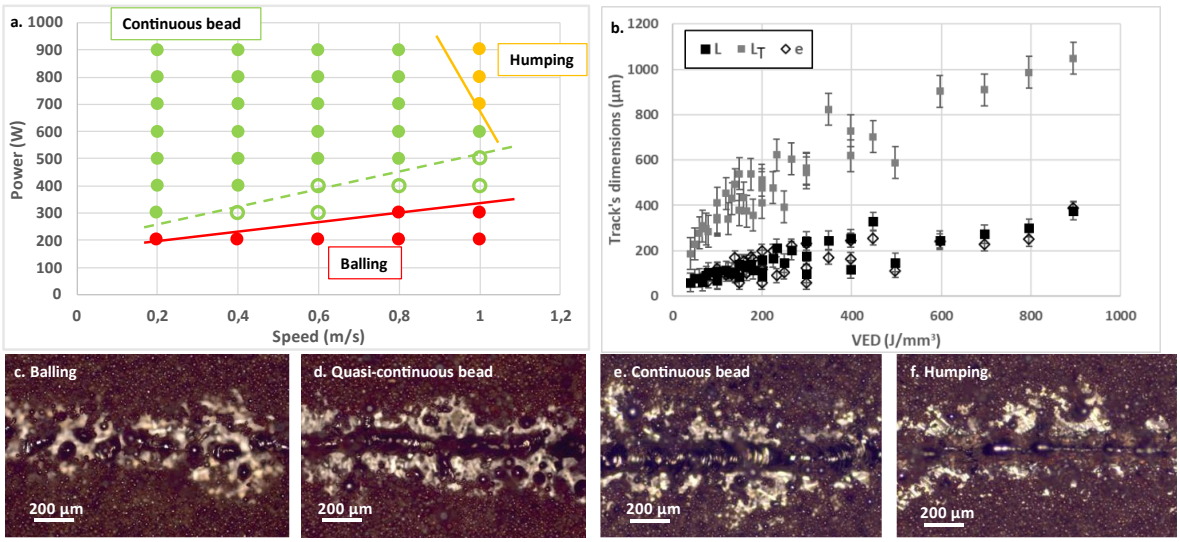

Fig. 3. (a) P-V stability charts for single tracks on a 70 µm powder thickness; (b) Measured: total affected width La, track width Lc, and depth penetration e; (c) Top view of a balling condition; (d) Top view of a quasi-continuous track condition; (e) Top view of a continuous track condition; (f) Top view of a humping condition.

- Track's widths and denudation areas

Measurements presented in Fig3(b) logically show a quasi-linear increase of tracks' width with the volume energy density (VED), considered as VED = P/(VxS) with S= spot area (mm²). Globally, widths are comprised between 100 and 200 µm for VED < 300 J/mm^3 and can reach up to 400 µm at a very high VED (900 J/mm^3). If we now consider the denudated area on each side of the track which is as large as track width, the total affected width affected by the tracks (La) is 3 times larger than the track width itself (Fig.3c).

- Penetration depth

An interesting point is that, contrary to usual L-PBF materials, the aspect ratio of tracks (depth over width) is always close to 1 (Fig.3b), even when a deep keyhole mode is shown. For instance, at VED = 140 J/mm^3, e ~ L ~ 110 µm. Comparatively, similar L-PBF conditions carried out on an Inconel 625 alloy (k= 15 W/m/K) provide much larger track volumes and aspect ratio, with e ~ 300 µm, L ~ 140 µm. Such small aspect ratios are mostly due to the very high thermal conductivity of Cu.

3.2. Impact of parameters on 3D parts density

Most of the 3D parts (cubic samples of 10 mm x 10 mm or 15 mm x 15 mm surface with variables heights between 4 mm and 12 mm) have been manufactured in the 80-230 J/mm^3, except one test at 390 J/mm^3. All the trials were made, with the same hatch and powder thickness Δh (=60 µm), and various power and speed. Corresponding conditions (P=300-1000 W, V=0.2-1 m/s) are comprised in the continuous and quasi-continuous zone of the single bead stability diagram (Fig.3a). For such conditions, the maximum productivity p* = Hatch x V x Δh obtained in the current work varies from 6 cm^3/h to 26 cm^3/h.

Last, a similar scanning strategy was used for all the parts, with a 90° rotation angle between subsequent layers. Finally, the Porosity versus VED data is reported in fig.4.

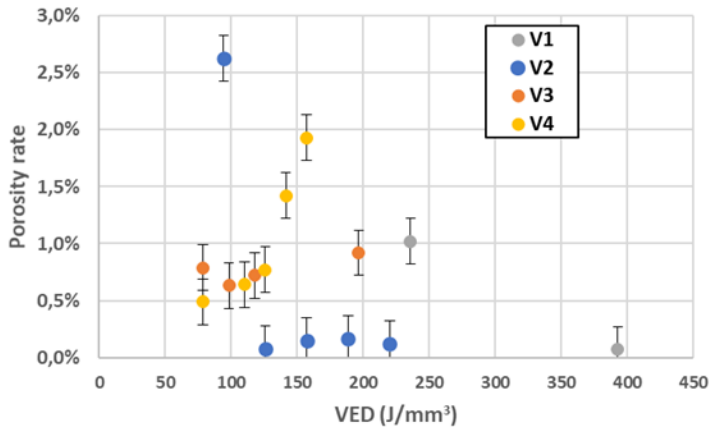

Fig.4. Porosity rate versus VED obtained on 3D cubic parts builds at the same hatch and layer thickness (60 µm). Four scan speeds are used with V1 < V2 < V3 < V4.

First, optimum L-PBF conditions (at V1 and V2 scan speed) allow obtaining less than 0.1 % porosity rate, which is, to our knowledge, the best porosity rate obtained ever on pure copper.

A second interesting aspect is that at the same energy level, increasing speed has a detrimental effect on porosity rates. For instance, for the same VED of 120 J/mm^3 an increase of speed results in an increase of the porosity rate (from 0.1 % at V2 to 0.75 % at V4). Another interesting point is that an increase of laser power at high speed (V> 0.5 m/s) also has a detrimental effect on a part's density. This is rather surprising considering results obtained on single tracks, which indicate large increases of the penetration depth and tracks width when the energy density increase. So, we should have expected a better remelting of the preview layer and a reduction of the porosity with the laser power increase. Such a result could be attributed to a deterioration of the building surface finish (more spatters, more humps) at high laser power and high speed, resulting in some lack of fusion. More specifically, this could be due to excessive local variation of the powder thickness for the next layer.

Finally, these preliminary tests at 515 nm indicate that it is not possible to use more than a maximum scan speed value to create dense parts. It is therefore difficult to increase productivity by increasing the speed even with higher powers while maintaining a similar energy density.

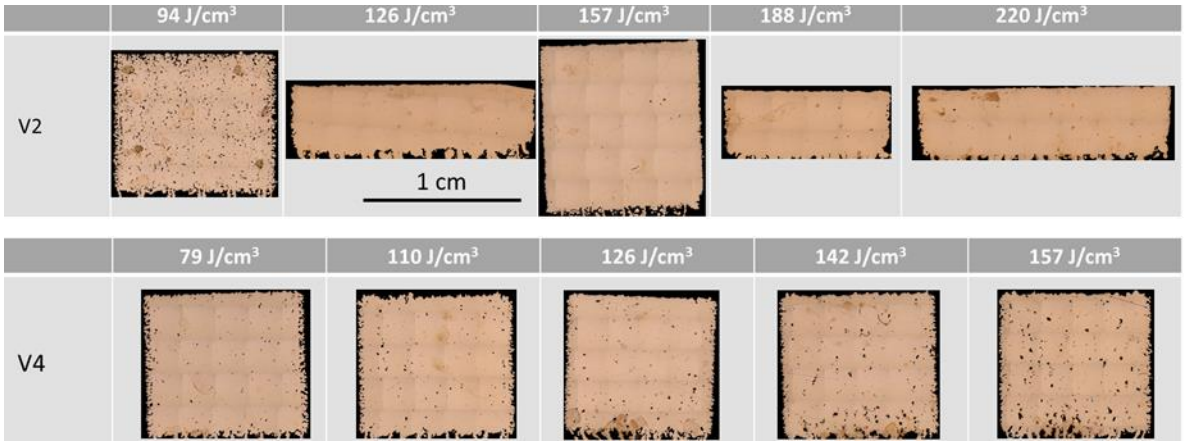

Fig.5. Cross-sections of 3D parts obtained for two scan speeds at various volume energy densities. Optimum densities are obtained for V2.

Due to the limitation on speed, the best way to enhance productivity would be to use larger hatch distances. For instance, considering either a 160 J/mm^3 energy density or a 300 J/mm^3 VED energy for a single track (at the same speed), the track's width increases from ~ 130 µm to ~$300\ \mu m$. Considering a similar overlap, hatch value and productivity could be doubled while maintaining the same porosity rate on the part. The maximum productivity p* defined by V*h*Δz could reach up to 32 cm^3/h with an increase of hatch and power.

3.3. Microstructures of 3D parts

Chemical etching and EBSD scans have been carried out to characterize the microstructure of the samples. Fig. 6 shows two different microstructures (Fig.6 a and b) obtained with two distinct VED values (122 J/mm^3 and 245 J/mm^3). For the denser part (Fig.6a,b), a strongly oriented <001> columnar microstructure is observed with a prominence of coarse elongated grains of more than 100 µm length. Large columnar grains are separated by smaller and vertically oriented grains, corresponding to the cooling of the center of individual tracks. The presence of these columns is standard for materials from SLM and discussed in detail by previous papers (Andreau et al., 2019) obtained for other and more classical L-PBF materials. The final texture observed is the result of the overlap of adjacent tracks.

For the less dense material shown in Fig.6(c), the occurrence of large porosity (50 to 100 µm) tends to stop the columnar texture, by interrupting the epitaxial growth. This results in a more equiaxed and finer grain structure, with grains' sizes varying between 10 µm and 100 µm. Physically, such an equiaxed structure is expected to come from a lack of metallurgical continuity and low dilution values.

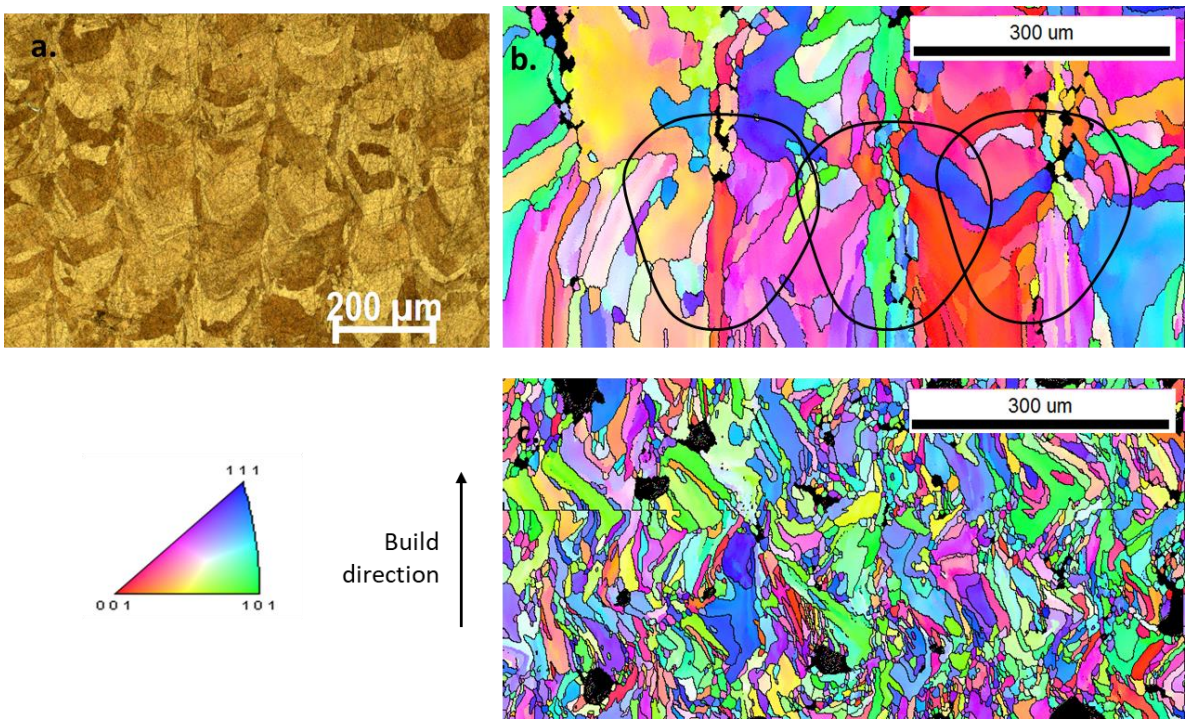

Fig.6. (a) Optical micrograph of an L-PBF cross-section obtained apart with a large track overlap; (b-c) EBSD analysis of L-PBF samples obtained with a green wavelength: (b) Large track overlap (VED = 252 J/cm^3); (c) Low track overlap (VED = 126 J/cm^3).

Conclusion

The present work has highlighted several key points to create dense parts using a green laser source.

First, a (P, V) process stability map was obtained on single L-PBF tracks to limit the range of P-V values. The penetration depth and track's width were also systematically measured to define process parameters. An interesting point is that, due to the high thermal conductivity of pure copper, the aspect ratio between penetration depth and track's width remained approximately the same (close to 1).

It was finally shown that a 515 nm wavelength – 1 kW output power source adapted on an L-PBF experimental testbench could allow building ~ 99.9% parts density with a maximum productivity rate of 32 cm^3/h. However, it was found a scan speed limit above which the building of 3D parts becomes detrimental for the same incident Volumetric Energy Density. This result has a direct implication on process productivity but could be counterbalanced by a better optimization of hatch distances in future works.

Last, classical L-PBF microstructures – oriented towards building direction- were shown of dense copper part, whereas low-density material was more equiaxed.

Future work will focus on a more detailed microstructural investigation together with the analysis of electrical conductivity and its dependence on porosity rate.

Acknowledgments

The authors thank all the people from the PIMM laboratory and AddUp for their support and assistance This work is carried out as part of the AMbition FUI project supported by BPI, Auvergne-Rhône-Alpes, and Ile-de-France regions.

References

Andreau, O., Koutiri, I., Peyre, P., Penot, J.-D., Saintier, N., Pessard, E., De Terris, T., Dupuy, C., Baudin, T., 2019. Texture control of 316L parts by modulation of the melt pool morphology in selective laser melting. Journal of Materials Processing Technology 264, 21–31. https://doi.org/10.1016/j.jmatprotec.2018.08.049

Colopi, M., Caprio, L., Demir, A.G., Previtali, B., 2018. Selective laser melting of pure Cu with a 1 kW single mode fiber laser. Procedia CIRP 74, 59–63. https://doi.org/10.1016/j.procir.2018.08.030

Colopi, M., Demir, A.G., Caprio, L., Previtali, B., 2019. Limits and solutions in processing pure Cu via selective laser melting using a high-power single-mode fiber laser. Int J Adv Manuf Technol 104, 2473–2486. https://doi.org/10.1007/s00170-019-04015-3

Engler, S., Ramsayer, R., Poprawe, R., 2011. Process Studies on Laser Welding of Copper with Brilliant Green and Infrared Lasers. Physics Procedia 12, 339–346. https://doi.org/10.1016/j.phpro.2011.03.142

Gunenthiram, V., Peyre, P., Schneider, M., Dal, M., Coste, F., Fabbro, R., 2017. Analysis of laser–melt pool–powder bed interaction during the selective laser melting of a stainless steel. Journal of Laser Applications 29, 022303. https://doi.org/10.2351/1.4983259

Haubold, M., Ganser, A., Eder, T., Zäh, M.F., 2018. Laser welding of copper using a high power disc laser at green wavelength. Procedia CIRP 74, 446–449. https://doi.org/10.1016/j.procir.2018.08.161

Heider, A., Hess, A., Weber, R., Graf, T., 2011. Stabilized copper welding by using power modulated green and IR laser beams, in: International Congress on Applications of Lasers & Electro-Optics. Presented at the ICALEO® 2011: 30th International Congress on Laser Materials Processing, Laser Microprocessing and Nanomanufacturing, Laser Institute of America, Orlando, Florida, USA, pp. 395–402. https://doi.org/10.2351/1.5062263

Jadhav, Dadbakhsh, Vleugels, Hofkens, Puyvelde, Yang, Kruth, Humbeeck, Vanmeensel, 2019. Influence of Carbon Nanoparticle Addition (and Impurities) on Selective Laser Melting of Pure Copper. Materials 12, 2469. https://doi.org/10.3390/ma12152469

Jadhav, S.D., Dadbakhsh, S., Goossens, L., Kruth, J.-P., Van Humbeeck, J., Vanmeensel, K., 2019. Influence of selective laser melting process parameters on texture evolution in pure copper. Journal of Materials Processing Technology 270, 47–58. https://doi.org/10.1016/j.jmatprotec.2019.02.022

Jadhav, S.D., Vleugels, J., Kruth, J., Van Humbeeck, J., Vanmeensel, K., 2020. Mechanical and electrical properties of selective laser-melted parts produced from surface-oxidized copper powder. Mat Design & Process Comms 2. https://doi.org/10.1002/mdp2.94

Kaiser, E., Dold, E.-M., Killi, A., Zaske, S., n.d. Application benefits of welding copper with a 1 kW, 515 nm continuous wave laser 6.

Lykov, P.A., Safonov, E.V., Akhmedianov, A.M., 2016. Selective Laser Melting of Copper. MSF 843, 284–288. https://doi.org/10.4028/www.scientific.net/MSF.843.284

Tang, C., 2020. Physics of humping formation in laser powder bed fusion. International Journal of Heat and Mass Transfer 18.